Vol. 1, No. 1, August 2022, pp. 41-54
p-ISSN: 2963-8577
DOI: 10.57102/jescee.v1i1.10

EFFECTS OF FLOW RATE AND INLET TEMPERATURE ON PERFORMANCE OF ANNULUS TYPE LOW-TEMPERATURE LATENT HEAT THERMAL ENERGY STORAGES

Rifki Yusup[1*] and Byan Wahyu Riyandwita[1]
[1]Department of Mechanical Engineering, Faculty of Industrial Technology, Universitas Pertamina, Indonesia

Abstract
Solar energy is one of the largest energy potentials which can be utilized in solar heater and integrated with the latent heat energy storage (LHTES). This research aims to investigate the effects of the operating conditions of flow rate and inlet temperature on the performance of the annulus type Low-Temperature LHTES using Computational Fluid Dynamics method in which the enthalpy-porosity is used as the solidification model. The results indicated that better performance can be obtained by increasing the flow rate and inlet temperature. The increase in flow rate resulted in a higher heat transfer, producing better performance up to 11.91% and 24.91% during the charging and discharging, respectively. Meanwhile, increasing the inlet temperature in the Low-Temperature LHTES system enhanced the performance up to 192.72% during the charging and 13.07% during the discharging.

Keywords:
Thermal storage; low-temperature LHTES; heat transfer performance; enthalpy-porosity; numerical simulation

Article History:
Received: July 31st, 2022
Revised: August 7th, 2022
Accepted: August 25th, 2022
Published: August 31st, 2022

Corresponding Author:
Rifki Yusup
Department of Mechanical Engineering, Universitas Pertamina, Indonesia
Email:
rifki.yusup@outlook.com

1. Introduction

The need of global energy has been increasing exponentially since the 1900s as depicted in Fig. 1 [1]. Considering the Paris Agreement in 2015, the world has started to see the potential of renewable energy to reduce fossil fuel emissions [2]. The largest renewable energy potential in Indonesia is solar with 207.8 GWp [3]. However, for harvesting solar energy, one of the biggest challenges is the intermittent characteristics of solar energy or only can be harvested in a limited period and in a fluctuated nature, as shown in Fig. 2 [4]. The use of the renewable energy worldwide is still low due to the imbalance of energy supply and demand period. Currently, the technology of energy storages such as sensible heat energy storages, latent heat energy storages, and chemical energy storages have been developed to solve the problem in the most effective, efficient, and safest way [5, 6].

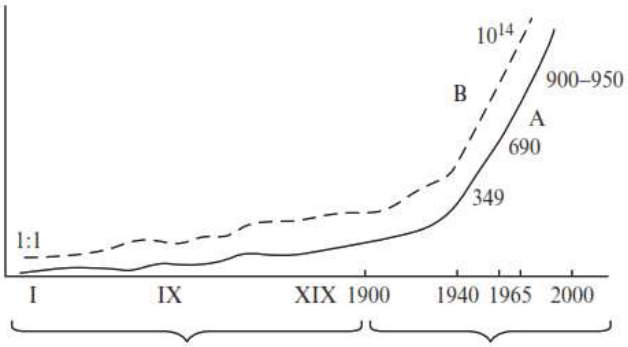

Figure 1. Global Energy Consumption [1]

Scapino, et. al. [7] reviewed that the latent heat thermal energy storages (LHTES) is one of the technologies that could achieve the three indicators explained before. LHTES is more effective in cost, has a high efficiency, and has a minimum response time [7]. Almost all LHTES applications have the same phase change material (PCM) geometry configuration of doughnut-shape, where the PCM will cover the tube in which heat transfer fluid is flowing inside the tube, as shown in Fig. 3 a) [5, 8–10]. One of methods to improve the thermal performance can be done by extending the heat transfer area and by making the fluid flows more turbulent [11, 12], by changing

the geometry configuration of the PCM, where the heat transfer fluid covers the annulus tube that contains the PCM.

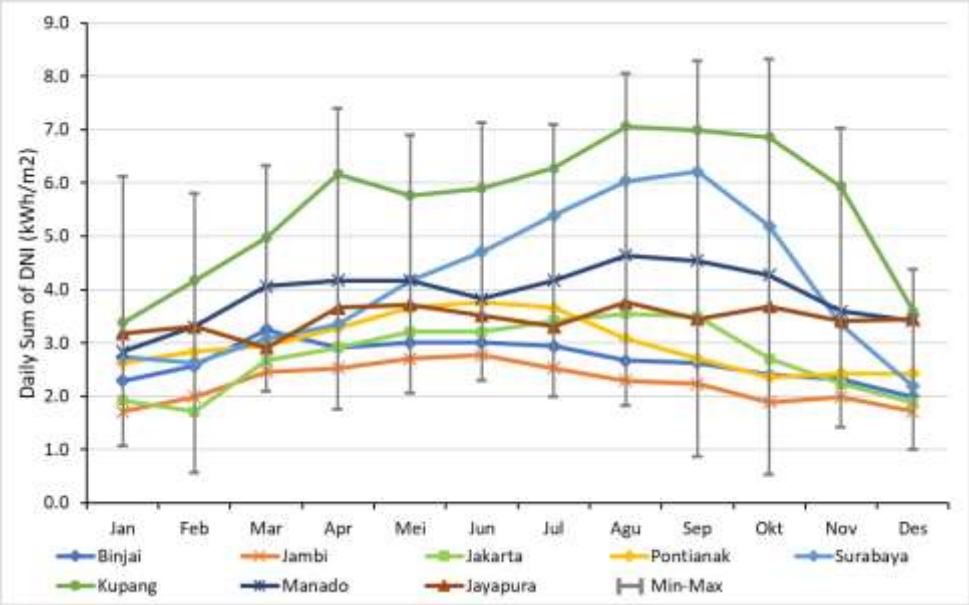

Figure 2. The Average of Daily Direct Normal Irradiance in a Few Cities in Indonesia [4].

Based on the applications, LHTES relies on the PCM or material for absorption of the thermal energy (heat storage) and classified as Low-Temperature (below 150°C, like for solar heater), Medium-Temperature (between 150°C-400°C), and High-Temperature (above 400°C, for Concentrated Solar Power, Steam Power Plant, etc.) applications [6, 13]. In this study, low temperature LHTES is selected for solar applications by using paraffin wax like *n*-octadecane for the PCM and evaluated in charging and discharging region because the properties of paraffin wax have a high density, stability of termal properties, unreactive, and the most important is the cycle resistance up to 2000 cycles [14, 15].

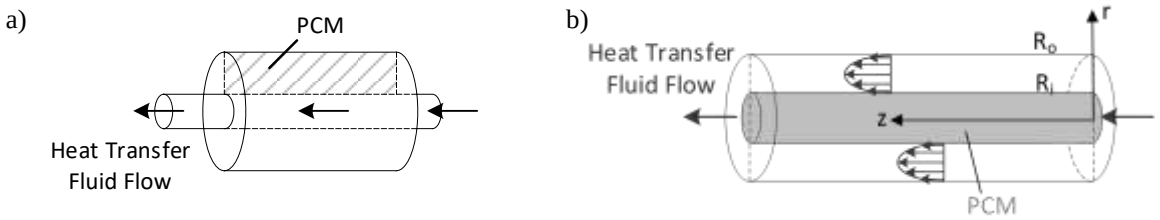

Figure 3. The Schematic Diagram of LHTES in a Geometry of
a) Doughnut Type (Shell-and-tube); and b) Annulus-tube.

2. Model Formulation

Here, the PCM is placed in the inner tube and the heat transfer fluid (HTF) flows through a pipe in the outer side of tube and cover the PCM tube (shell-side) with adiabatic wall as depicted in Fig. 3 b). Various configuration of inlet temperature and flow rate of HTF are considered in this research. The evaluation of performance of charging and discharging is evaluated by enthalpy of the process.

A. Governing Equations

The governing equations are employed for two components, water and PCM. During charging, the water, which flows in the outer side tube, transferred the heat to melt the PCM and stored the thermal energy in a liquid phase. While during discharging, the heat that stored in PCM is then taken by the cold water and thus solidified the PCM. In this research, a three-dimensional model is simplified into two-dimensional to reduce the cost of computation.

In the HTF, the convection of heat and fluid flow will be considered by using the Navier-Stokes equations. These equations focused on conservation of mass, momentum, and energy [5, 9].

$$\frac{\partial \rho}{\partial t} + \nabla.(\rho \boldsymbol{u}) = 0 \tag{1}$$

$$\frac{\partial(\rho \boldsymbol{u})}{\partial t} + \nabla.(\rho \boldsymbol{u_r} \boldsymbol{u}) + \rho[\omega \times (\boldsymbol{u} - \boldsymbol{u_t})] = -\nabla p \boldsymbol{I} + \nabla.[\mu(\nabla \boldsymbol{u} + (\nabla \boldsymbol{u})^T)] + \rho \boldsymbol{g} \tag{2}$$

$$\frac{\partial(\rho\, c_p\, T)}{\partial t} + \nabla.\left(\rho\, \boldsymbol{u_r}\, c_p\, T\right) = \nabla.(k\, \nabla T) \tag{3}$$

During the process of melting and solidification, the molten PCM will form a mushy zone where it will decrease the value of porosity. To evaluate solidification process, the enthalpy-porosity formulation is represented as a source term, $\boldsymbol{S}_{mom}$, and it is added to the conservation momentum Equation (2) with the value defined as:

$$\boldsymbol{S}_{mom} = \frac{(1-\beta)^2}{(\beta^3 + 1 \times 10^{-3})} \times \zeta\, \boldsymbol{u} \tag{4}$$

where, ζ is mushy zone constant that has value of $1{\times}10^{5}$` for *n*-octadecane.

Then, the enthalpy is added on energy conservation Equation (3) and defined as

$$H_{pcm} = \widetilde{h_{pcm}} + \widetilde{\Delta H_{pcm}} \tag{5}$$

where, $\widetilde{h_{pcm}}$ is sensible heat of PCM and defined as:

$$\widetilde{h_{pcm}} = \widetilde{h_{pcm,ref}} + \int_{Tref}^{T} C_{p,pcm} \tag{6}$$

where, $\widetilde{h_{pcm,ref}}$ is reference enthalpy on reference temperature and ΔH_{pcm} is latent heat of PCM which is a function of liquid fraction, β of the PCM.

$$\widetilde{\Delta H_{pcm}} = \beta.L \tag{7}$$

B. Constitutive Relations

The water liquid defines as HTF that has temperature dependent polynomial functions for the thermophysical properties. The density, viscosity, and thermal conductivity of water are defined in (8-10) respectively. The other thermophysical properties are presented in Table 1.

$$\rho_w = -3.570 \times 10^{-3}\, T^2 + 1.88\, T + 753.2 \tag{8}$$

$$k_w = -8.354 \times 10^{-6}\, T^2 + 6.53 \times 10^{-3}\, T - 0.5981 \tag{9}$$

$$\mu_w = 2.591 \times 10^{-5} \times 10^{\frac{238.3}{T-143.2}} \tag{10}$$

The PCM (*n*-octadecane) also has temperature dependent polynomial functions for the thermophysical properties that are defined in (11-13) and the other properties are presented in Table 1.

$$\rho_{pcm} = \frac{774}{9 \times 10^{-4}(T - 300.65) + 1} \tag{11}$$

$$k_{pcm} = \begin{cases} 0.358, & T < T_s \\ 126.421 - 0.42T, & T_s \le T \le T_l \\ 0.148, & T > T_l \end{cases} \tag{12}$$

$$\mu_{pcm} = 0.001 \times \exp\left(-4.649 + \frac{1.79 \times 10^3}{T}\right) \tag{13}$$

To evaluate the heat transfer rate, $\dot{Q}$ on charging and discharging condition can be evaluated by

$$\dot{Q}_{transfer,} = \frac{H_{pcm}}{t_{transfer}} \tag{14}$$

So, the efficiency of thermal enhancement ratio of heat transfer, *TER* can be determined by

$$TER = \frac{\dot{Q}_{transfer} - \dot{Q}_{transfer,base}}{\dot{Q}_{transfer,base}} \times 100\% \quad (15)$$

Table 1. Thermophysical Properties of Water Liquid and *n*-octadecane [9, 16].

Parameters	Value	Unit
Water Liquid		
Melting Temperature, $T_{m,w}$	273.15	K
Latent Heat, L_w	2100	J • kg^{-1}
Specific Sensible Heat, $C_{p,w}$	4200	J • kg^{-1} • K^{-1}
PCM (*n*-octadecane)		
Melting Temperature		
• Solidus Temperature, T_s	300.15	K
• Liquidus Temperature, T_l	300.65	K
Latent Heat, L_w	2.43×10^5	J • kg^{-1}
Specific Sensible Heat, $C_{p,pcm}$	2160	J • kg^{-1} • K^{-1}
Coefficient of Thermal Expansion	9.00×10^{-4}	K^{-1}

C. Boundary Conditions

In this research, these following boundary conditions are employed on the model.

- Inlet: at the inlet, a various inlet mass flow rate and inlet temperature is specified as shown in Table 2.
- Outlet: at the outlet, stream-wise gradient of temperature and gauge pressure are set to be zero.
- PCM wall is set to be no-slip condition, zero roughness height, and coupled
- HTF wall is set to be insulated wall (no heat flux), no-slip condition, and zero roughness height.

Table 2. Inlet Conditions.

Various Mass Flow Rate						**Various Inlet Temperature**					
Charging			***Discharging***			***Charging***			***Discharging***		
No	**$\dot{m}$ (kg/s)**	**T_c (K)**	**No**	**$\dot{m}$ (kg/s)**	**T_d (K)**	**No**	**$\dot{m}$ (kg/s)**	**T_c (K)**	**No**	**$\dot{m}$ (kg/s)**	**T_d (K)**
CF1	0.01575	310.65	DF1	0.01575	295.65	CT1	0.03150	305.65	DT1	0.03150	295.65
CF2	0.03150	310.65	DF2	0.03150	295.65	CT2	0.03150	310.65	DT2	0.03150	295.65
CF3	0.15750	310.65	DF3	0.15750	295.65	CT3	0.03150	320.65	DT3	0.03150	295.65

3. Numerical Methodology

In this research, the LHTES model and grid generation are conducted in ANSYS Workbench 2019 R2 in which simplified symmetrical 2D model is used as depicted in Fig. 4. Then, the mathematical model formulation (governing equations, constitutive relations, and boundary conditions) is implemented and solved. For several thermo-physical properties of HTF and PCM, the C-Language is coded and compiled for user-defined functions in the model.

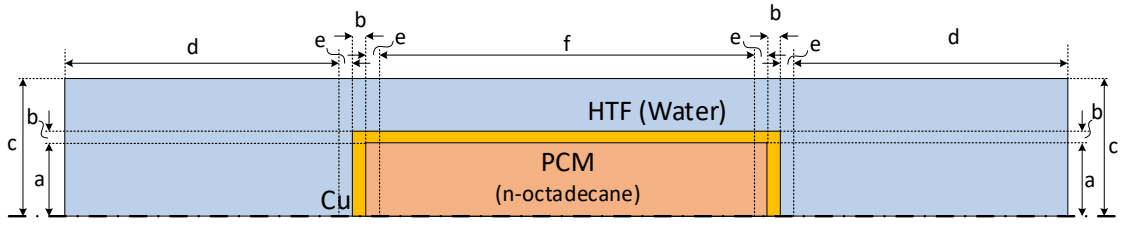

Figure 4. The Schematic Diagram of 2D Symmetrical Annulus-tube LHTES System.

To ensure the grid generation is independence, the grid independent study was conducted by dividing the domain into areas and set the number of divisions in c-side to increase the number of fluid elements (cells), the summary of the test shown in Table 3 and the results is presented in Fig. 5. It is seen that, there is no significant differences on the average liquid fraction of PCM due to the time which means the number of cells is not affecting the value significantly. Hence, the grid size of 71,568 cells was chosen for all cases of this study. The results of this grid is shows in Fig. 6 with the orthogonal quality is 0.9998 which means the setting of grid is good.

Semi-Implicit Pressure Linked Equation (SIMPLE) algorithm is chosen for solving the numerical model of this research. The momentum and energy equations are solved by the second order upwind discretization and pressure correction equation is adopted in the PRESTO! scheme. A time step of 0.1 second is taken with the number of maximum iterations of 20 times for each time step. Convergence criterion of 1×10^{-3} is selected for the momentum and turbulent equations and 1×10^{-5} is set for the energy.

Table 3. Grid Generation for Grid Independent Study.

No	Number of Partition*			Size of c-side* (mm)	Number of Elements (Cells)
	Area b	Area d	Area f		
1	6	80	800	1.00	57,960
2	6	100	1000	1.00	71,568
3	8	100	1300	1.00	88,368
4	8	150	1500	0.75	116,436
5	8	200	2000	0.75	153,760

Note: *Check the area *x* in Figure 4

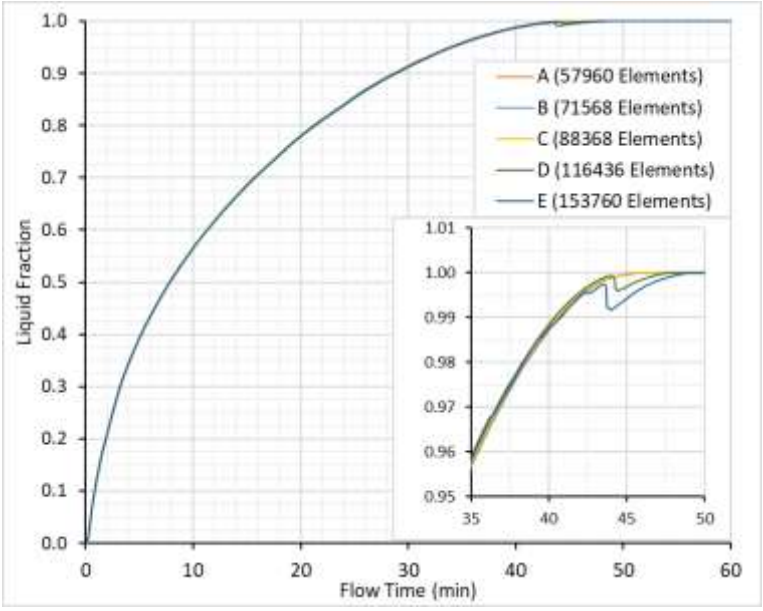

Figure 5. Comparison of Grid Independent Study.

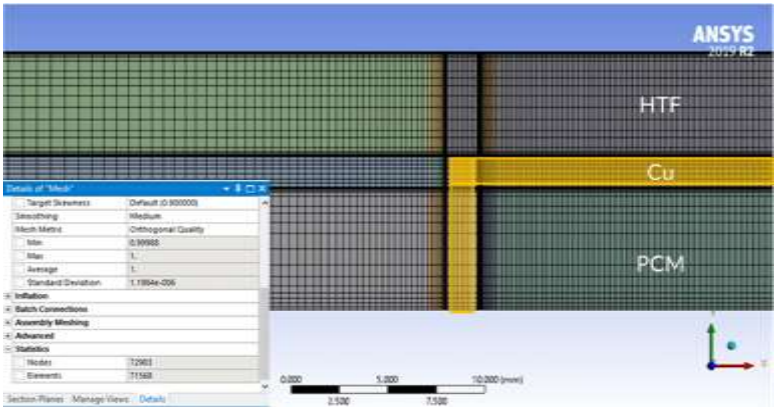

Figure 6. Detail Grid Result (71,568 cells in Total: Orthogonal Quality of 0.9998).

4. Results and Discussion

A. Model Validation

To ensure correct selection and settings of the mathematical model, the validation is made by comparing the results of the simulation with the results of previous experiment [8]. The comparison is focusing on two temperature locations (T_1 and T_2) and the results are shown in Fig. 7. As can be seen from Fig. 7, a relatively good behavior is shown with small relative error of 0.357% for T_1 and 0.152% for T_2. This explain that the settings and parameters of this research are valid and thus the simulation results sufficiently describe the behavior of the LHTES.

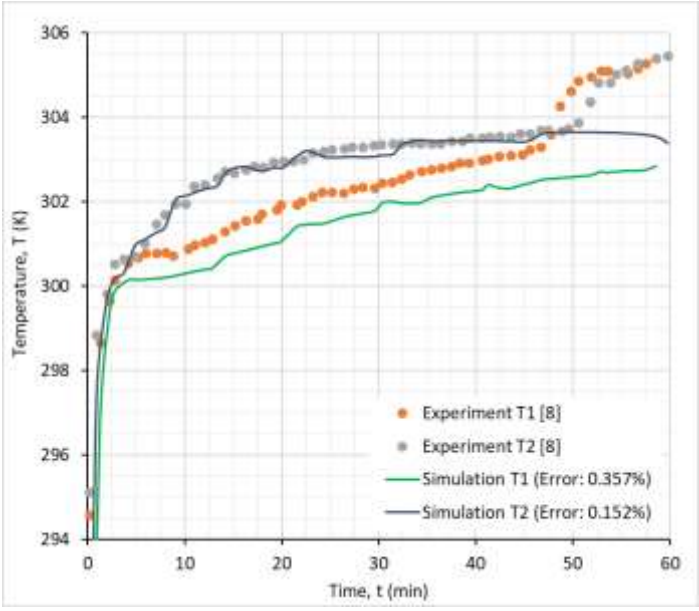

Figure 7. Comparison of Simulation and Experiment Results [8].

B. Effect of Mass Flow Rate

The heat transfer in LHTES is affected by the flow condition, especially flow rate. Hence, this research is carried out to prove and find the behavior of heat transfer of PCM in three variation flow rates of 0.01575 kg/s; 0.03150 kg/s; and 0.15750 kg/s. The simulation is evaluated by flowing the hot water with 310.65 K (10 K above the melting temperature of PCM, *n*-octadecane) in the inlet.

Fig. 8 presents the average PCM liquid fraction during charging-discharging process for the flow rate variation. This figure shown that from the initial until charging process ended, the increase of flow rate will increase the heat transfer rate. This is also implied that at higher flow rate the liquid fraction of PCM is faster to reach value of 1.0 which means the PCM has melted completely into the liquid phase. Higher flow rate creates more turbulence eddies. These eddies will mix the fluid elements and speed up the convection rate in the heat transfer process, thus give faster melting process in the PCM [17].

Fig. 8 also shows that the rate of liquid fraction is slower towards the end of charging cycle because the heat transfer in PCM is started to be dominated by convection process. This phenomenon also depicted in Figs. 9 and 10 where the melting process in the center region of the PCM is reduced due to the change of conduction process into a convection process near the wall. Figs. 9 and 10 also shows that towards the end of the charging cycle, the temperature of PCM will approach the hot water temperature and in the higher flow rate and the melted area in the PCM tends to be larger.

The behavior of flow rate effect on the discharging process is similar to the charging process. When the flow rate is increased, the solidification of PCM is increased because turbulence effect on heat transfer. Fig. 11 and 12 show that at higher flow rate, the area of solidification near the wall in PCM is larger and accompanied with lower temperature distribution.

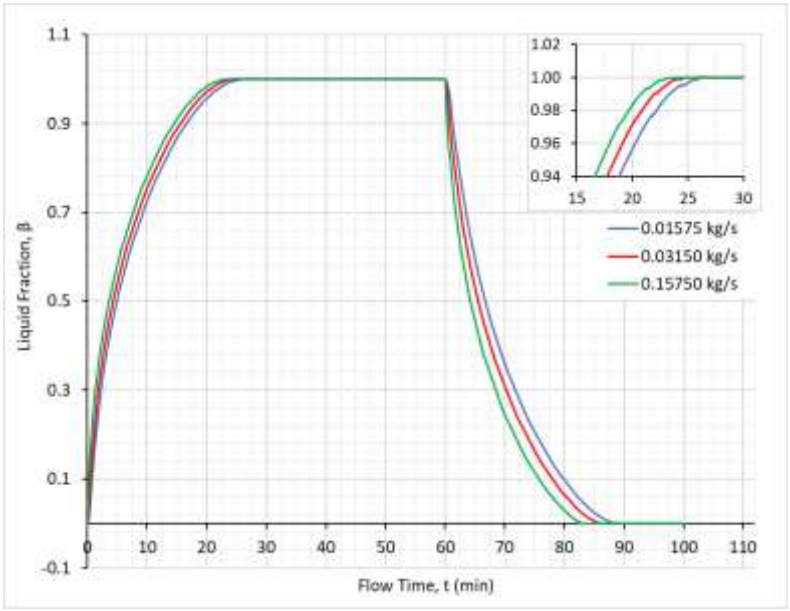

Figure 8. Average PCM Liquid Fraction during Charging and Discharging for Different Flow Rates.

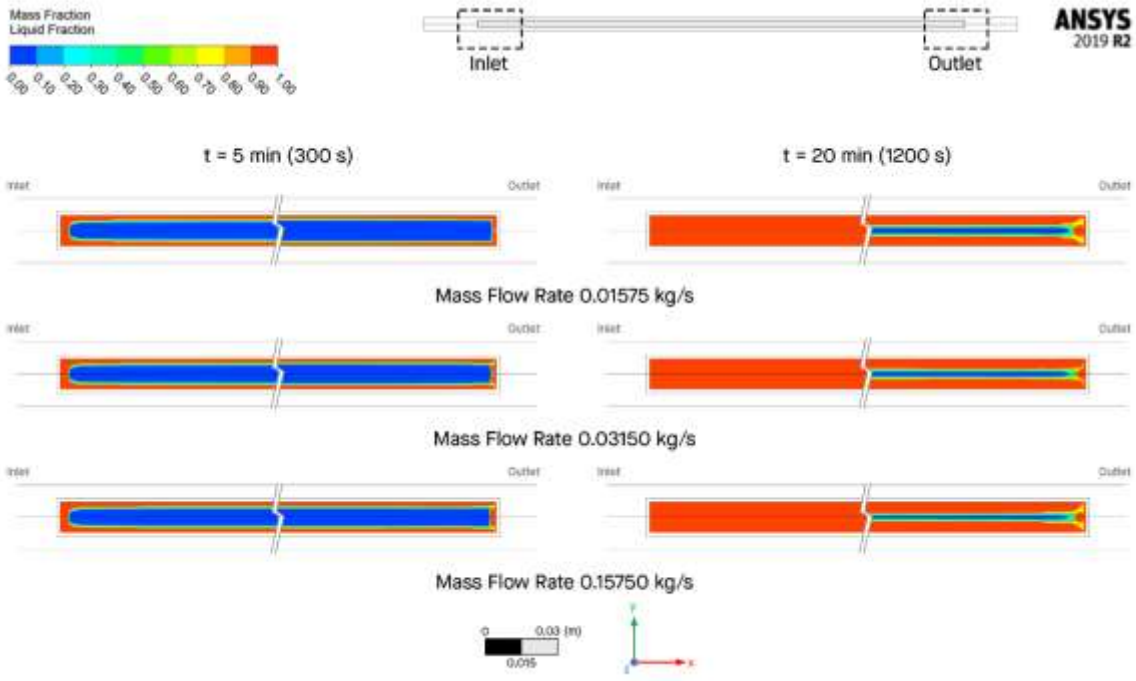

Figure 9. Comparison of Average PCM Liquid Fraction for Different Flow Rates at 5 mins and 20 mins (Charging).

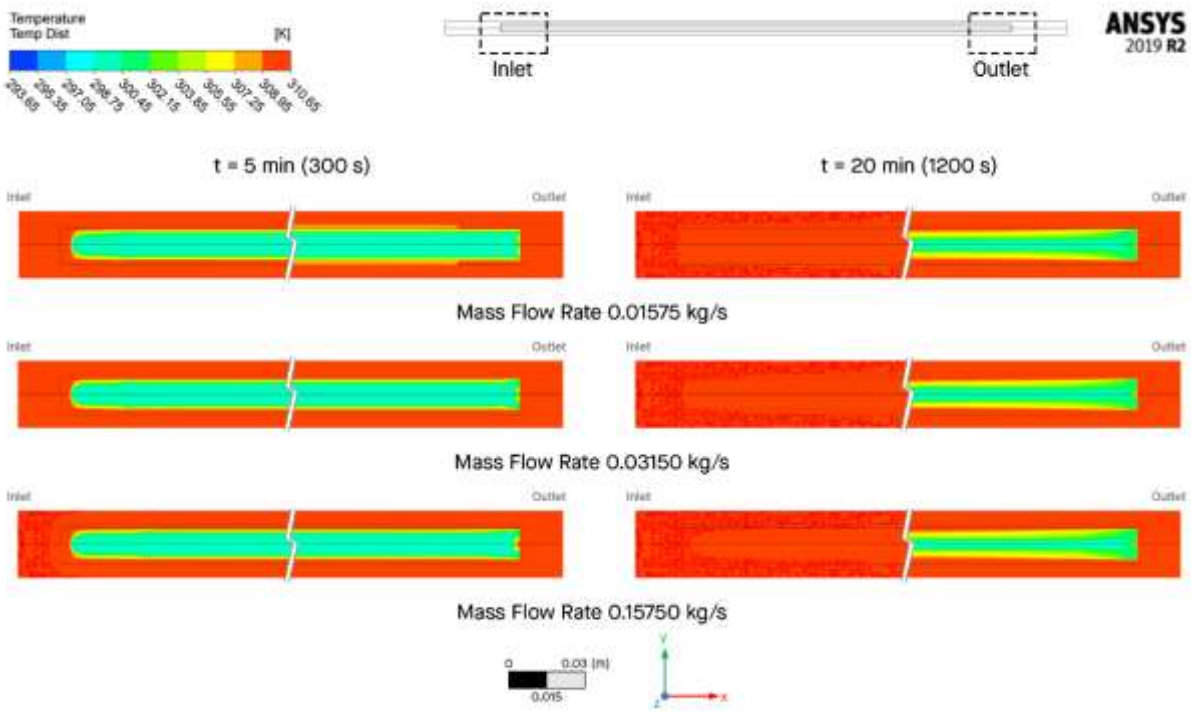

Figure 10. Comparison of Temperature Distribution for Different Flow Rates at 5 mins and 20 mins (Charging).

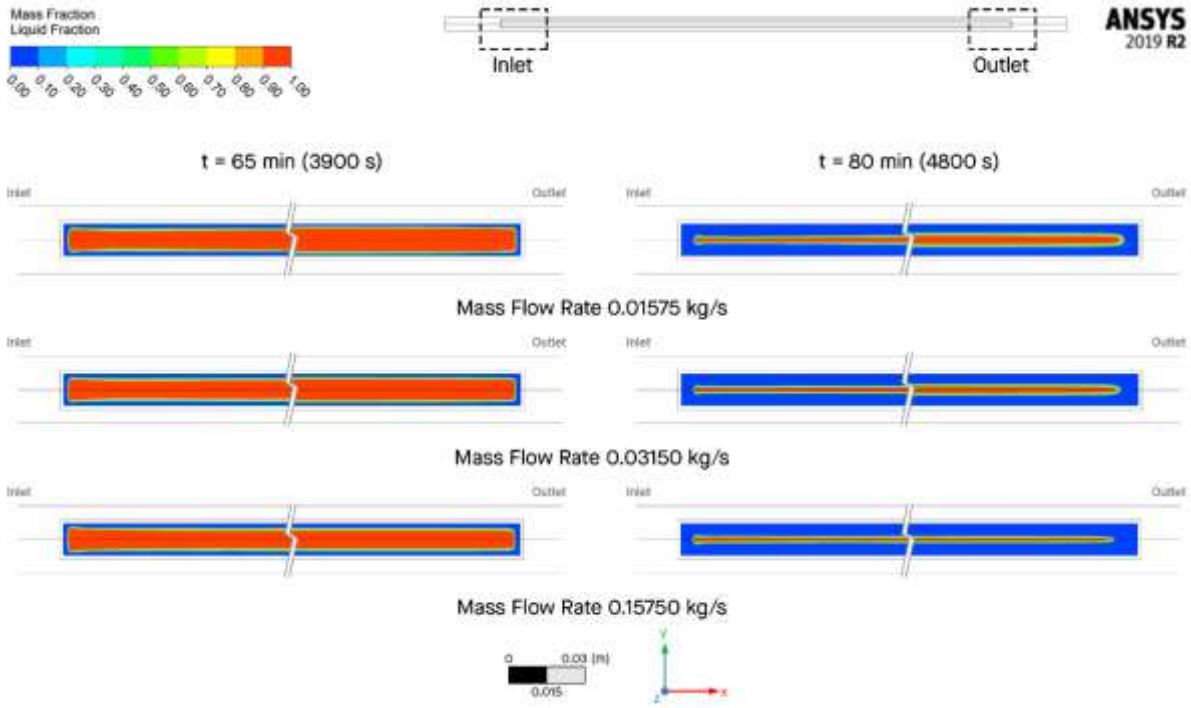

Figure 11. Comparison of Average PCM Liquid Fraction for Different Flow Rates at 65 mins and 80 mins (Discharging).

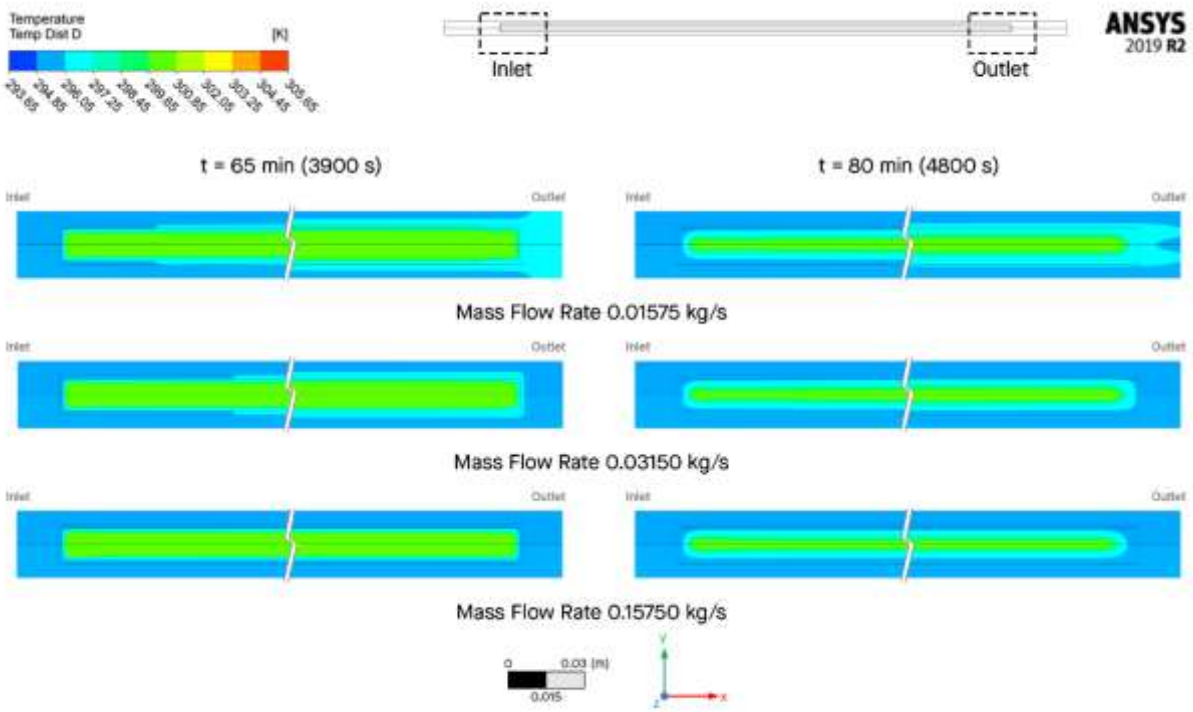

Figure 12. Comparison of Temperature Distribution for Different Flow Rates at 65 mins and 80 mins (Discharging).

Table 4 is the summary for the evaluation of the overall heat transfer performance (Thermal Enhancement Ratio, TER) for each case. The value shows that by increasing the flow rate the heat transfer process will be faster. Increasing 2 times the flow rate will give 6.17% and 10.90% higher efficiency of heat transfer on charging and discharging, respectively. Meanwhile, increasing 10 times of the flow rate will improve the efficiency by 11.91% in charging and 24.91% in discharging.

Table 4. Heat Transfer Enhancement due to Flow Rate.

Mass Flow Rate, (kg/s)	Heat Transfer Rate (W)		Thermal Enhancement Ratio (%)	
	Charging	Discharging	Charging	Discharging
0.01575 (*base*)	15.251	-14.662	0.00	0.00
0.03150	16.193	-16.260	6.17	10.90
0.15750	17.068	-18.314	11.91	24.91

C. Effect of Inlet Temperature

The inlet temperature gives more significant effect towards the average PCM liquid fraction as depicted in Fig. 13, especially during the charging process. As can be seen from Fig. 13, the heat transfer rate increases as the inlet temperature of the HTF increases and promotes faster melting processes of the PCM. Figs. 14 and 15 shows supporting evidence for this tendency that in the fifth minute of charging, the PCM is melted in the area near wall and the area of liquid PCM is larger at the higher temperature water. The similar behavior also depicted at the 20th minute of charging. Thus, with increasing of the inlet temperature of HTF, the temperature difference will also increase and will drives the heat transfer process both by conduction (in the solid state) and convection (in the liquid state) faster [8, 18] and gives higher trend of the curve gradient.

During discharging process, it shows slightly different behavior from the charging one. Fig. 13 shows the rate of the average PCM liquid fraction during discharging is almost similar or looks like there is no effect by the temperature variation. The temperature and liquid fraction distribution that shown in Figs. 16 and 17 respectively also shows almost no differences due to the inlet temperature. However, if the graphs in Fig. 13 are enlarged in Fig. 13, the curve with 320.65 K was reaching the zero liquid fraction which slightly faster than the other two which indicate that the heat transfer process for 320.65 K slightly faster than the others.

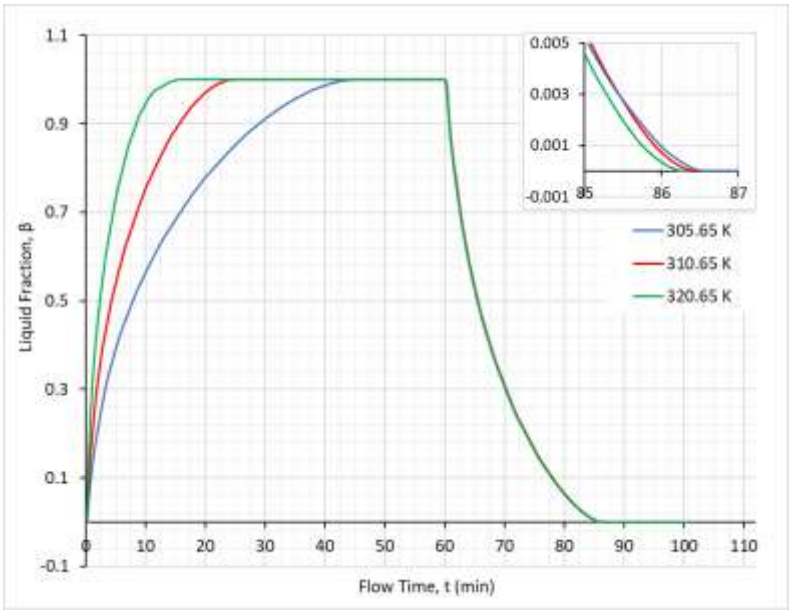

Figure 13. Average PCM Liquid Fraction during Charging and Discharging for Different Inlet Temperature.

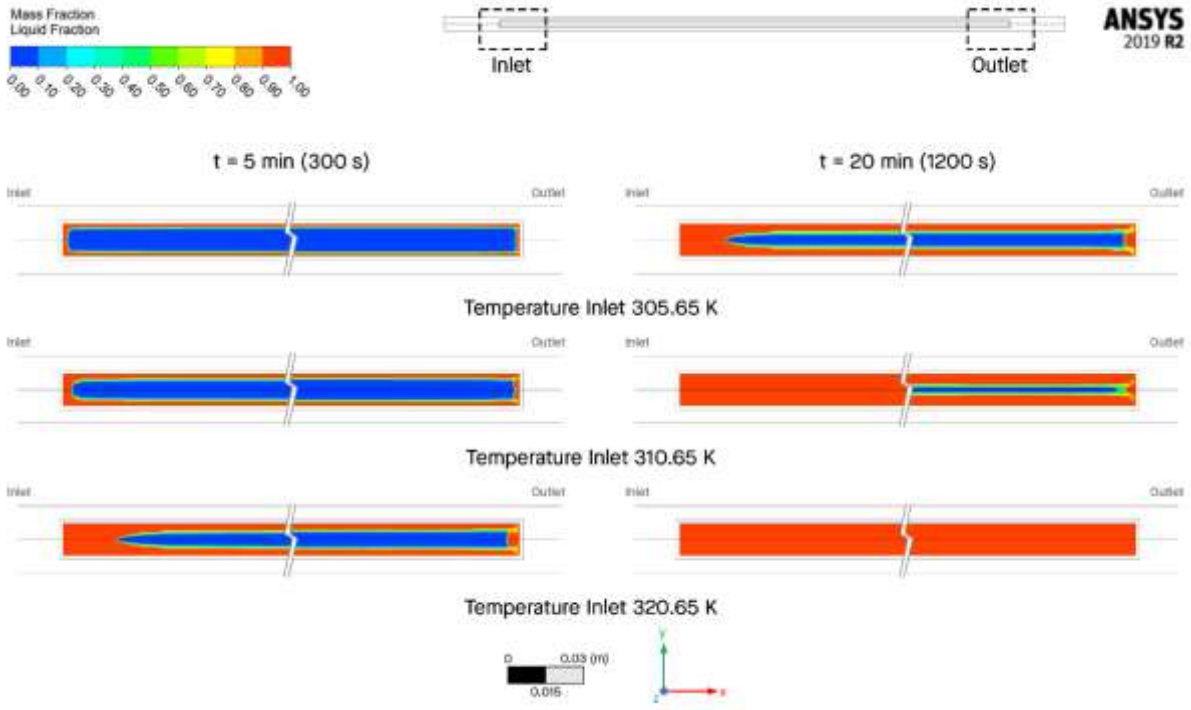

Figure 14. Comparison of Average PCM Liquid Fraction for Different Inlet Temperature at 5 mins and 20 mins (Charging).

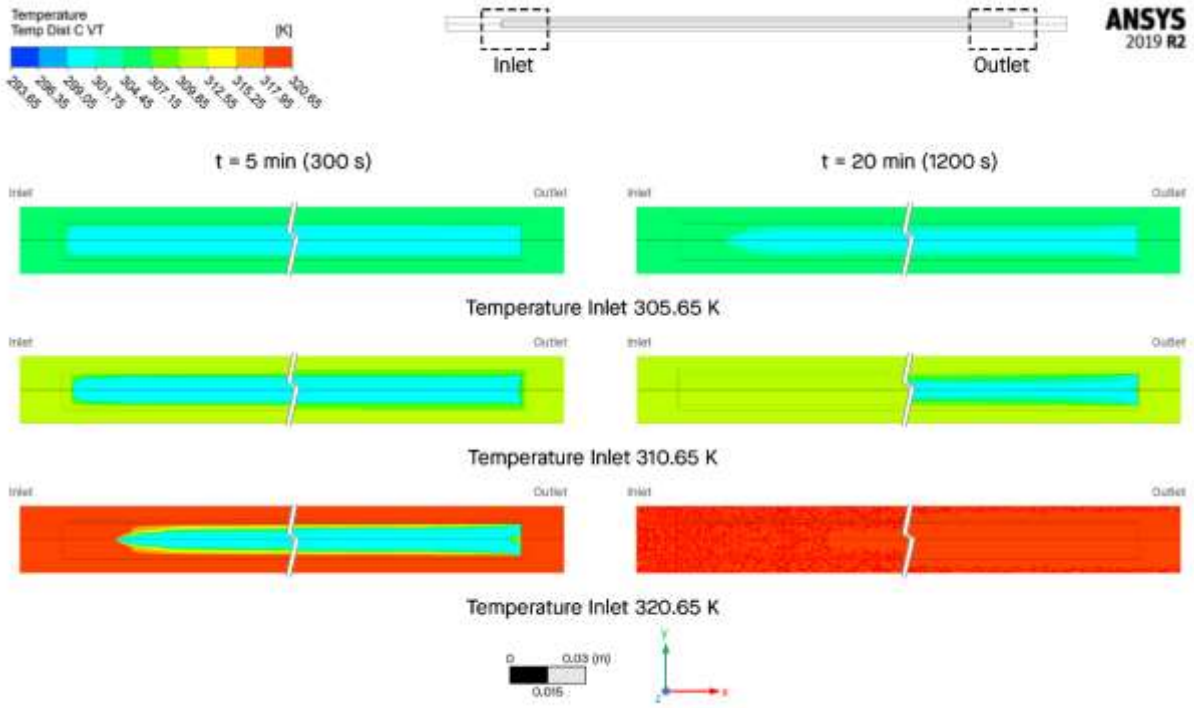

Figure 15. Comparison of Temperature Distribution for Different Inlet Temperature at 5 mins and 20 mins (Charging).

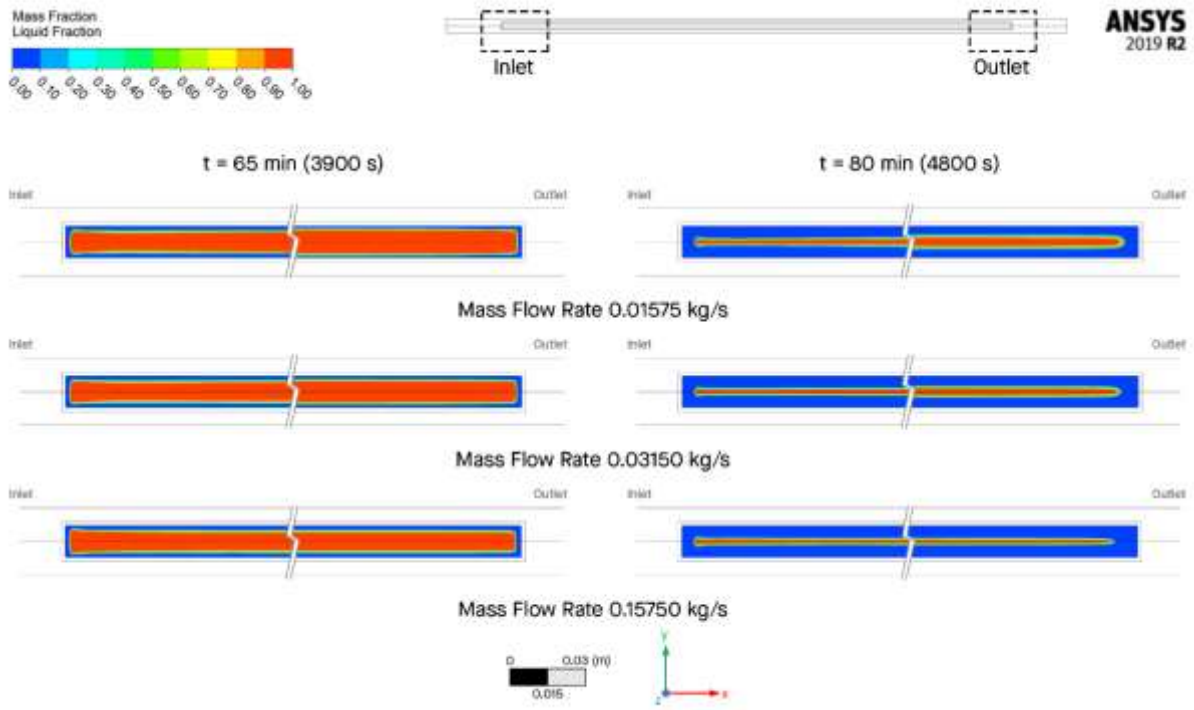

Figure 16. Comparison of Average PCM Liquid Fraction for Different Inlet Temperature at 65 mins and 80 mins (Discharging).

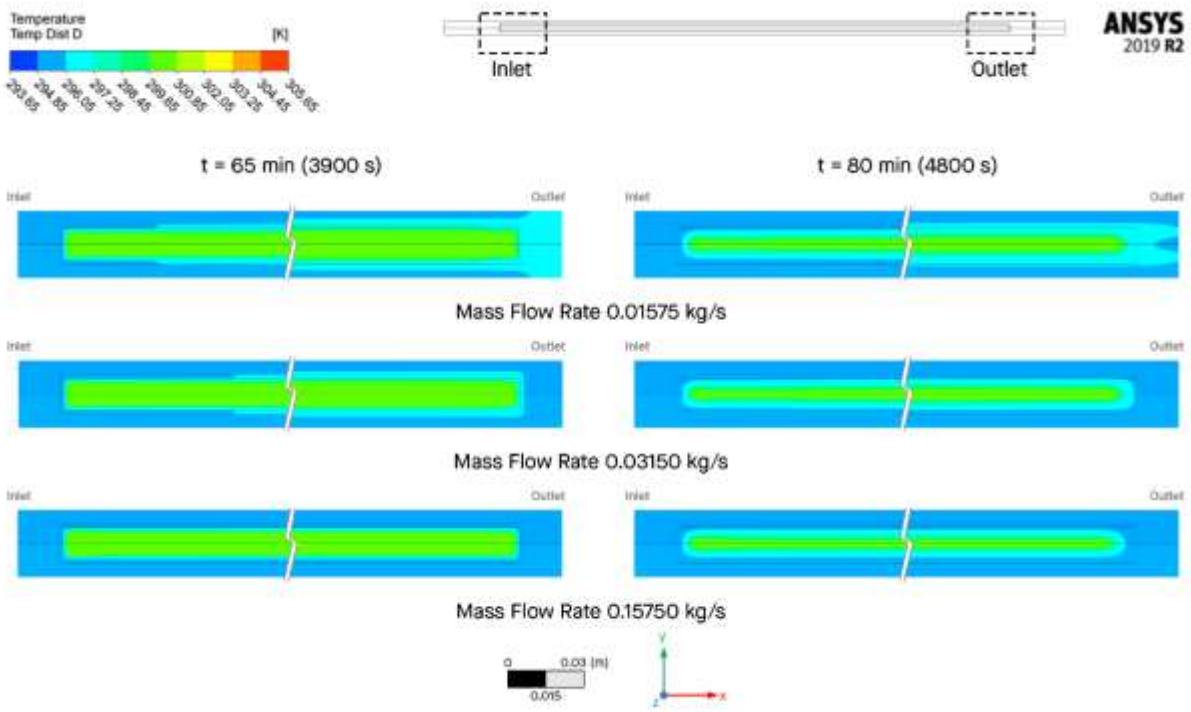

Figure 17. Comparison of Temperature Distribution for Different Inlet Temperature at 65 mins and 80 mins (Discharging).

Looking at the heat transfer performance for different inlet temperatures, as summarized in Table 5, it is found that the inlet temperature will gives relatively a higher effect on the heat transfer performance (thermal enhancement ratio, TER) especially during charging cycle. The highest temperature (adding 20 K above the melting point of PCM) will give relatively a higher heat transfer performance up to 192.72% during the charging and 13.07% during the discharging.

Table 5. Heat Transfer Enhancement due to Inlet Temperature.

Inlet Temperature (K)	Heat Transfer Rate (W)		Thermal Enhancement Ratio (%)	
	Charging	Discharging	Charging	Discharging
305.65 (*base*)	8.898	-15.573	0.00	0.00
310.65	16.193	-16.260	81.98	4.41
320.65	26.047	-17.609	192.72	13.07

5. Conclusions

Based on this numerical simulation, the behavior of flow rate and inlet temperature on annulus type LHTES with *n*-octadecane as PCM could give significant effect in the heat transfer performance, both during charging and discharging process.

- Maximizing the flow rate could give more turbulence effect on LHTES system so it could speed up the heat transfer process. In this research, increasing the flow rate 10 times will give 11.91% and 24.91% efficiency during charging and discharging respectively.
- Rising the inlet temperature will give more significant temperature difference and drives the heat transfer process. By setting the temperature 10 K above melting point of PCM could give the efficiency of heat transfer up to 192.72% during charging and 13.07% during discharging.
- Based on the characteristics above, preferred thermal performance could be designed by carefully at first evaluate the operating condition of the inlet temperature and then followed by the flow rate.
- This research also imply that the annulus-type could be applied on Low-Temperature LHTES system.

References

[1] A. Ter-Gazarian, "Energy Storage for Power Systems," *The Institution of Engineering and Technology*, 2011.
[2] C. Strinati and R. Ferroukhi, Renewable Energy and Climate Pledges: Five Years After the Paris Agreement, Abu Dhabi: International Renewable Energy Agency, 2020.
[3] D. Siswanto, Outlook Energi Indonesia 2019, Jakarta: Sekretariat Jenderal Dewan Energi Nasional, 2019.
[4] Solargis, Solar Resource and Photovoltaic Potential of Indonesia, Washington DC: The World Bank, 2017.
[5] J. C. Kurnia, A. P. Sasmito, J. S. V. and A. S. Mujumdar, "Improved Design for Heat Transfer Performance of a Novel Phase Change Material (PCM) Thermal Energy Storage (TES)," Applied Thermal Energy, pp. 896-907, 2013.
[6] A. Crespo, C. Barreneche, M. Ibarra and W. Platzer, "Latent Thermal Energy Storage for Solar Process Heat Appliacations at Medium-High Temperature - A Review," Solar Energy, pp. 1-32, 2018.
[7] L. Scapino, H. A. Zondag, J. V. Bael, J. Diriken and C. C. Rindt, "Sorption Heat Storage for Long-term Low-temperature Applications: A Review on The Advancements at Material and Prototype Scale," Applied Energy, pp. 920-948, 2017.
[8] M. Lacroix, "Numerical Simulation of a Shell-and-Tube Latent Heat Thermal Energy Storage Unit," Solar Energy, pp. 357-367, 1993.
[9] J. C. Kurnia and A. P. Sasmito, "Numerical Investigastion of Heat Transfer Performance of Rotating Latent Heat Thermal Energy Storage," Applied Energy, pp. 1-13, 2017.
[10] D. Li, Y. Hu, D. Li and J. Wang, "Combined-Cycle Gas Turbine Power Plant Integration with Cascaded Latent Heat Thermal Storage for Fast Dynamic Responses," Energy Conversion and Management, pp. 1-13, 2019.
[11] F. Yuan, M.-J. Li, Z. Ma, B. Jin and Z. Liu, "Experimental Study on Thermal Performance of High-Temperature Molten Salt Cascaded Latent Heat Thermal Energy Storage System," International Journal of Heat and Mass Transfer, pp. 997-1011, 2018.
[12] T. Istanto and W. E. Juwana, "Pengujian Karakteristik Perpindahan Panas dan Faktor Gesekan pada Penukar Kalor Pipa Kosentrik dengan Sisipan Pita Terpilin Berlubang," Mekanika, pp. 7-14, 2011.
[13] A. Shukla, D. Buddhi and R. Sawhney, "Solar Water Heaters with Phase Change Material Thermal Energy Storage: A Review," Renewable and Suistanable Energy Reviews, no. 13, pp. 2119-2125, 2009.
[14] S. P. Jesumathy, M. Udayakumar and S. Suresh, "Heat Transfer Characteristics in Latent Heat Storage System Using Paraffin Wax," Journal of Mechanical Science and Technology, no. 3, pp. 959-965, 2012.
[15] P. J. S. Siagian, Desain Thermal Energy Storage Tipe Shell-and-Tube pada Thermal Heat Energy Storage dengan Material Parafin Wax RT-55 sebagai Phase Change Material, Yogyakarta: Universitas Gadjah Mada, 2019.
[16] "PubChem Compound Summary for CID 11635, Octadecane," 2020. [Online]. Available: https://pubchem.ncbi.nlm.nih.gov/compound/Octadecane. [Accessed 1 August 2020].
[17] R. Winterton, "Fusion Reactors," in Thermal Design of Nuclear Reactors, Oxford, Pergamon, 1981, pp. 163-172.
[18] T. L. Bergman, A. S. Lavine, F. P. Icropera and D. P. Dewit, Fundamentals of Heat and Mass Transfer, Jefferson City: John Wiley & Sons, 2011.

Biographies of Authors

Rifki Yusup, S.T. is currently an engineer at one of oil and gas company and has graduated his bachelor's degree from Department of Mechanical Engineering, Universitas Pertamina, Jakarta, Indonesia in 2020.

Byan Wahyu Riyandwita, S.T., M.Eng., Ph.D. is currently a lecturer who focus on thermal-fluid modeling at Departement of Mechanical Engineering, Universitas Pertamina, Jakarta, Indonesia and has finished his doctoral degree program from Gyeongsang National University in 2011.